Hindawi
Advances in Civil Engineering
Volume 2019, Article ID 8131052, 15 pages
https://doi.org/10.1155/2019/8131052

Research Article

Rotation Stiffness Investigation of Spatial Joints with End-Plate Connection

Shizhe Chen,[1] Jianrong Pan,[2,3] Zhan Wang,[2,3] and Chao Zhou[4]

[1]*School of Civil and Transportation Engineering, Guangdong University of Technology, Guangzhou 510006, China*
[2]*Department of Civil Engineering, South China University of Technology, Guangzhou 510640, China*
[3]*State Key Laboratory of Subtropical Building Science, South China University of Technology, Guangzhou 510640, China*
[4]*Department of City and Environment Science, City College of Dongguan University of Technology, Dongguan 523419, China*

Correspondence should be addressed to Zhan Wang; wangzhan@scut.edu.cn

Received 21 May 2019; Revised 12 September 2019; Accepted 16 September 2019; Published 30 October 2019

Academic Editor: Flora Faleschini

Spatial joints with end-plate connections show significant spatial coupling effects under spatial loading. Mechanical behaviour and failure modes of these spatial joints differ from those of planar joints. This study involved experiments and finite element analyses with respect to planar joints with end-plate connections under static load. The numerical results agreed well with the experimental data, and this verified the adequacy of the finite element analyses. Then, finite element models of the spatial interior joint, exterior joint, and corner joint were established to analyse the difference between the mechanical behaviour of spatial joints and planar joints. The component method was used to analyse components contributing to the initial stiffness of spatial joints. An initial rotation stiffness calculation model of spatial joints was proposed based on the deformation of joints. The findings indicated that results of the calculation models were in good agreement with those of the finite element analyses, and this proved that the calculation model proposed in this study could act as a reference method.

1. Introduction

Joints are an important part of an entire structure. Some previous studies [1, 2] examining beam-column connections focused on in-plane behaviour. However, the actual loading state of the joint should be spatial. The behaviour of the frame structure joints depends on the combined effect of the major-axis and minor-axis connections. Only planar connections were considered in actual structural design, and this does not reflect the actual mechanical behaviour of joints. Thus, it is necessary to separately consider coupling effects under spatial loading.

The moment-rotation behaviour of the end-plate joint with an extended stiffener was investigated by Tartaglia et al. [3, 4], and also, the design method was developed by Francavilla et al. [5]. Katalin and Miklós [6] investigated a modified component method that could be applied to the analysis of spatial joints. Cabrero and Bayo [7, 8] investigated the connection behaviour of a new spatial joint subjected to proportional spatial loading. Simoes da Silva [9] presented a conceptual design model of spatial joints. This conceptual design model was a combination of the calculation models of spatial joints based on the component method principle. Loureiro et al. [10] investigated spatial joints with end-connections on the major axis and minor axis. The results indicated that minor-axis connections offered a higher degree of improvement to the rotation stiffness of the joints when compared with that of major-axis connections. Gil et al. [11] used an experimental study and finite element analyses to investigate the interaction between major-axis and minor-axis connections of spatial joints. Zhou [12] conducted a set of experiments with respect to spatial composite joints.

Researchers also developed simplified models and calculation methods of initial rotation stiffness of planar joints, such as modifying the component method [13], application of new joints [14], and new loading condition [15]. The component method in the Eurocode was the most widely

used analytical method. However, a few studies investigated the initial rotation stiffness of spatial joints. Calculation models for the initial rotation stiffness of steel joints loaded along the major axis were provided by EC3 [16], which were only applied to planar joints. The interaction stiffness effect between the major axis and minor axis was not investigated before. And, this effect could not be neglected in mechanical behaviour research of spatial joints.

This study investigated the rotation stiffness of the spatial joints considering the interaction stiffness effect between the major axis and minor axis. The accurate finite element modelling method was proposed by comparing the resultant curves with static experiments of planar joints. Finite element models of spatial joints were then constructed based on the verified modelling method. Differences in the initial rotation stiffness between spatial joints with end-plate connections and planar joints were evaluated. The theoretical rotational stiffness calculation method of the spatial joint was developed, and the result proved to be accurate.

2. Experimental Tests on the Joint Stiffness

Two kinds of specimens were designed. These joints were designed according to the code for design of steel structure [17], and the dimension was referenced from a practical engineer of an automobile repair workshop. According to the code, the column web and flange were designed to satisfy the shear deformation of the panel zone, and for the connection along the minor axis, the thickness of the column was increased to enhance the mechanical performance of the panel zone. The first specimen involved a major-axis interior joint with an extended end-plate connection that was numbered as MZ-1. The other specimen involved a minor-axis interior joint with flush end-plate connections that was numbered as MZ-2. Figure 1 shows the details of the panel zone.

The dimensions of the triangular stiffener on the right beam of MZ-1 corresponded to $75\,\text{mm} \times 75\,\text{mm} \times 10\,\text{mm}$ (Table 1). Both columns and beams were composed of hot-rolled H-section steel with a strength grade of Q235B. The test mainly includes planar joints under symmetric loading and the material quality testing of the components. The properties of components are listed in Table 2. The high-strength bolt is of 10.9 grade, and the material property of the bolt was referenced from Guo [18] and listed in Table 3. Different connection types on the left and right of the joints were labelled as the left connection and right connection, respectively.

Figure 2 presents the test setup and details of the material test. A reaction frame and a distributive beam were used to fix the top of the column, and a hydraulic jack was used to support the other end. It should be noted that it was necessary for the point of the resultant force of the hydraulic jack and the loading beam to coincide with the centroid of the column. Synchronized loads were applied to both ends of the beams. An oil distributor system was adopted to guarantee the synchronization of loading. Additionally, brackets were installed close to both ends of the beams to prevent lateral buckling.

The entire loading process involved unidirectional symmetric loading, and the specific loading process is as follows: (1) The column was first subjected to a prescribed axial force (axial compressive ratio = 0.3) corresponding to $0.3 f_y A_s$, where f_y and A_s denote the design strength of steel and the cross-section area of the column, respectively. (2) The ends of the beams were then subjected to unidirectional symmetric forces. Force control was employed prior to the yielding of the specimens. Following this, displacement control was applied at the ends of beams until there was local buckling at the upper flange of the beam, and the specimens could not continue to bear the load.

Mechanical parameter results are provided in Table 4. The moment-rotation response for all specimens is illustrated in Figure 3. Figure 3(a) shows that large differences existed between the left connection and right connection. These differences were attributed to the stiffener in the end-plate of the right connection. The stiffener enhanced both bearing capacity and stiffness of the joint and guaranteed the rotation capacity of the joint. The test data of the minor-axis end-plate connection are shown in Figure 3(b). This study only presented the test results of the left connection because specimen MZ-2 was bilaterally symmetrical and under symmetric loads. Although the ends of the specimen were asymmetric due to the nonsynchronization of loading positions and loading processes, they were still controllable.

Wang and Wang [19] reported that the displacement of the beam end has a nonlinear relationship with the rotation angle. The displacement of the beam end in the elastic stage consists of the joint rotation angle and deflection of the beam itself. In the plastic stage, the effect of beam plastic deformation should be considered. Therefore, the moment-rotation relationship of the connection was calculated using the following equation:

$$s = \theta L + \frac{ML^2}{(3\text{EI})}, \qquad s = \theta L + \theta' L + \frac{ML^2}{(3\text{EI})}, \tag{1}$$

where s is the vertical displacement of the beam end, θ is the rotation angle of the beam to the column connection, θ' is the plastic rotation angle of the beam, M is the moment of the beam end, θL is the elastic deformation at the beam end in the elastic stage, $\theta' L$ is the plastic deformation at the beam end in the plastic stage, and EI is the bending rigidity of the beam.

3. Finite Element Model

A FE modelling software, ANSYS [20], was used to develop three-dimensional FE models of planar joints. The SOLID45 element was used to model the beams, columns, end-plates and bolts of the spatial joints. The element sizes of the bolts and the joint panel zone corresponded to 8 mm, and the element sizes of other parts were in the range of 20–30 mm. A surface-to-surface contact formulation was defined between the different parts of steel and between the bolts and the steel. The target faces and contact faces were modelled by the TARGE170

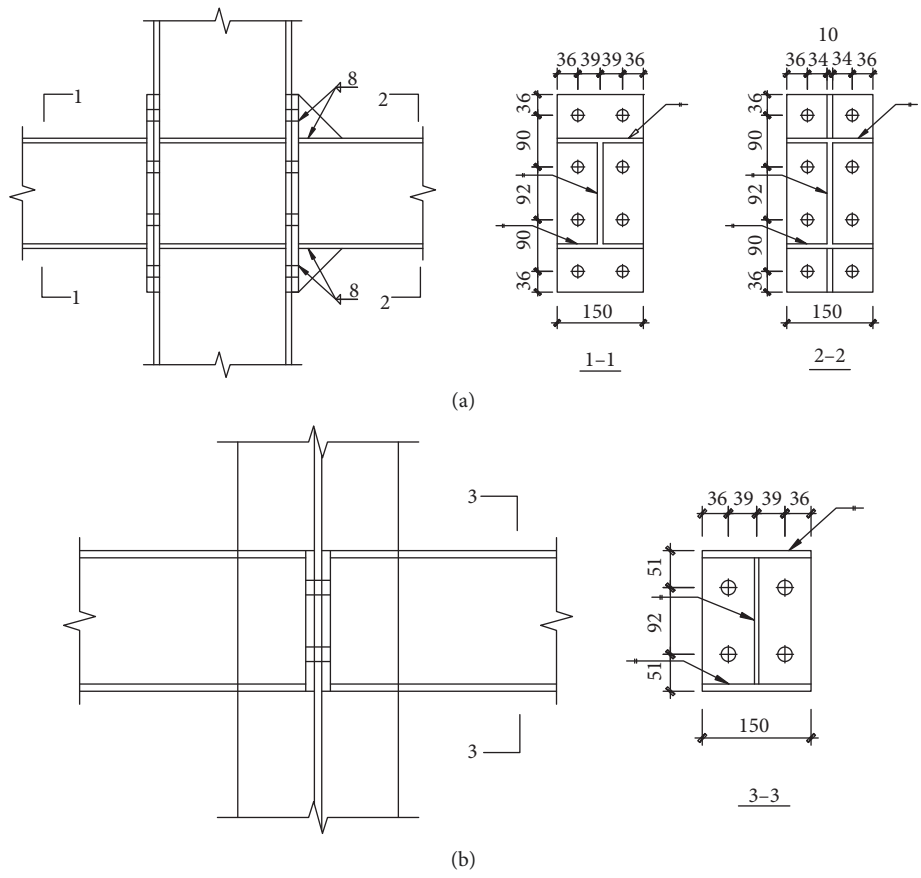

Figure 1: Details of the specimens. (a) MZ-1. (b) MZ-2.

Table 1: Geometric properties of the specimens.

Specimen label	Column dimension (mm)	Beam dimension (mm)	End-plate dimension (mm)	Bolt diameter (mm)
MZ-1	H244 × 175 × 7 × 11	H194 × 150 × 6 × 9	344 × 150 × 16	20 mm
MZ-2	H244 × 175 × 7 × 11	H194 × 150 × 6 × 9	194 × 150 × 16	20 mm

Table 2: Material properties of steel.

Component	Thickness (mm)	Yield stress f_y (MPa)	Tensile stress f_u (MPa)	Elastic modulus E (GPa)	Elongation (%)
Column web	7	263.5	467.0	205	22.0
Beam flange	9	262.4	435.3	196	22.7
Stiffener	10	241.8	384.3	208	25.0
Column flange	11	263.1	445.6	206	20.2
End-plate	16	251.6	405.8	196	26.0

Table 3: Material properties of the bolt.

High-strength bolt (Grade 10.9)	Yield stress f_y (MPa)	Tensile stress f_u (MPa)	Elasticity modulus E (GPa)	Yield strain ε_y
	940	1040	206	45.6

element and the CONTA174 element, respectively. The friction coefficient between the contact faces was 0.45.

The grade of the steel used was Q235B in which $f_y = 235$ MPa, according to the code for design of steel structure [17]. Tables 2 and 3 provide a summary of the material properties of the H-section steel and bolts. Considering that the high-strength bolt is less ductile as compared with the H-section steel and the yield stress of the high-strength bolt is much higher, two constitutive models were provided to describe the H-section steel and the bolt, respectively. A trilinear isotropic hardening model was used as the constitutive model of the H-section steel. Grade 10.9 (M20) high-strength bolts with a yield strength of 940 MPa were used. A bilinear kinematic hardening model was used as the constitutive model of the bolt, and the value of the modulus of the hardening stage was 10% of the elasticity modulus as shown in Figure 4. For the H-section steel,

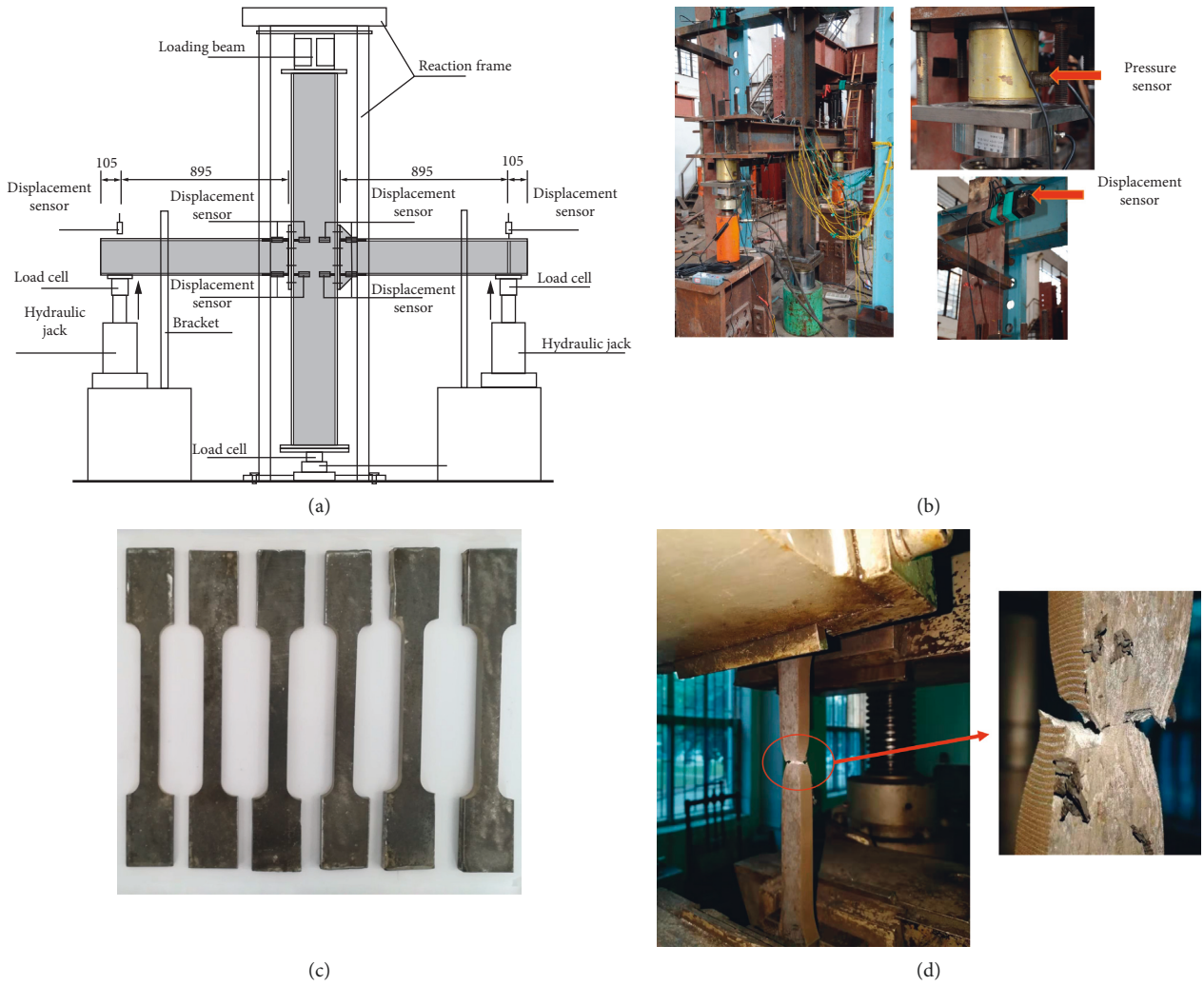

Figure 2: Test setup and the material test. (a) Joint of the interior column loaded. (b) Testing rig. (c) Material test samples. (d) Necking area.

Table 4: Test results.

Specimen	Position	Yield moment (kN·m)	Ultimate moment (kN·m)	Yield rotation (rad)	Initial rotation stiffness (kN·m·rad^{-1})	Max displacement of beam end (mm)	Max load of beam end (kN)	Failure pattern
MZ-1	Left connection	73.7	110.1	0.0081	9879	64	114	Buckling at flange, large deformation of end-plate
	Right connection	89.9	121.2	0.0072	13574	78	109	
MZ-2	Left connection	32.0	58.7	0.0035	9769	65	60	Pull crack of bolts, large deformation of end-plate
	Right connection	—	—	—	—	—	—	

$f_y = 260$ Mpa, $f_u = 436$ Mpa, $\varepsilon_y = 0.001327$, and $\varepsilon_u = 0.010306$. For the bolt, $f_y = 940$ Mpa, $f_u = 1040$ Mpa, $\varepsilon_y = 0.004563$, and $\varepsilon_u = 0.009417$.

Figure 5 shows the FE models and mesh division. The boundary conditions of the spatial joints in the FE model included fixing the bottom of the column and constraining the horizontal movement of the top of the column. An axial force with a value that was 0.3 times the yielding bearing capacity of the column cross-section was applied on the top of the column. The loading mode corresponded to symmetric loading at the ends of beams.

3.1. Comparison of the Test Results with Finite Element Analysis. Figure 6 shows the comparisons of the moment-rotation curves of specimen MZ-1 and specimen MZ-2. The

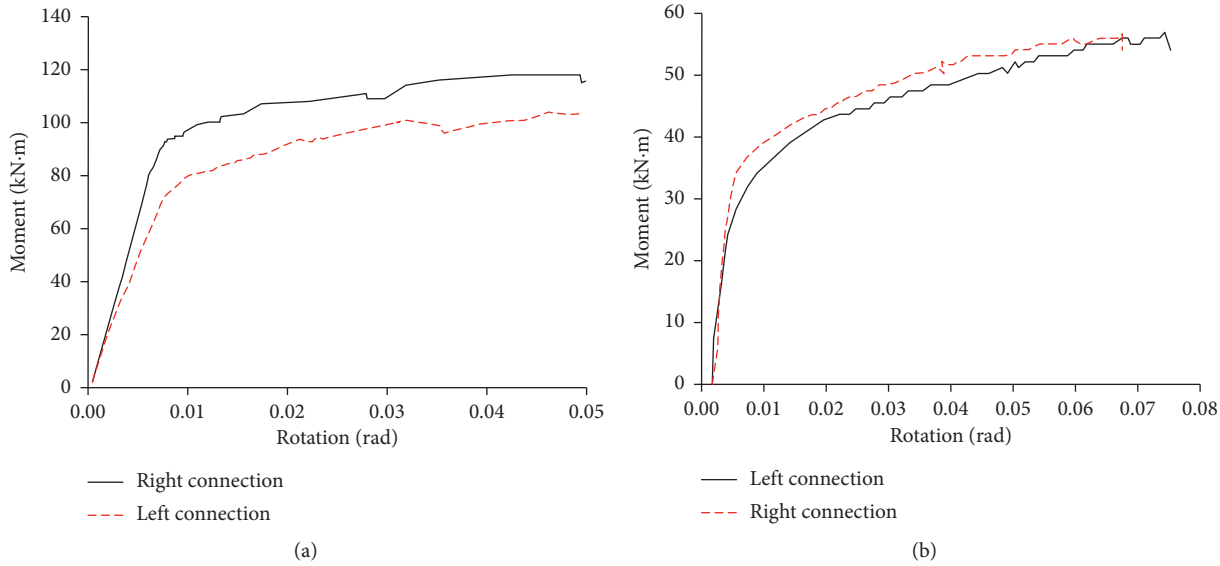

Figure 3: Moment-rotation curves for specimens. (a) Specimen MZ-1. (b) Specimen MZ-2.

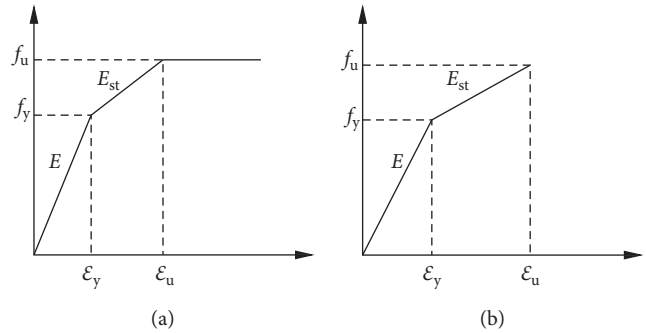

Figure 4: Constitutive model of materials. (a) Constitutive model of H-section steel. (b) Constitutive model of the bolt.

left connection curves were compared to illustrate the effectiveness of the FE simulation. It can be observed that there was good agreement between the test results and the FE simulation in the elastic stage. Additionally, in the stage after yielding, there was some disparity due to the simplification of the constitutive behaviour of the materials and test errors. As shown in Figure 7, the final deformations of the test specimens and the numerical simulation were in good agreement. According to the comparison of curves and deformations, this finite element model had been proven to be sufficiently accurate for simulating these planar joints (Figure 8).

3.2. FE Models of Spatial Joints. The joints can be classified as three types, namely, middle column joints, edge column joints, and corner column joints, as shown in Figure 9. Tables 5 and 6 list the specific sizes and labels of the FE models of planar joints and spatial joints, respectively.

3.3. Influence of Different Loading Modes. Spatial loading represents the loading mode that involved concentrated loads at the ends of the beams connected with the joint. Planar loading represents the loading mode that only included the action of unidirectional loading. In order to improve computation efficiency, the FE models of the middle column joints and the edge column joints could be reduced by half based on the structural forms and the force conditions. The FE models and the mesh division of the middle column joints, edge column joints, and corner column joints are shown in Figure 9.

Figure 10 shows comparisons of the moment-rotation curves of the major-axis connections of the spatial joints under spatial loading and planar loading, and Table 7 lists the mechanical properties of the joints. The elastic ultimate moment could be defined by the yielding of components such as a beam flange, beam web, column flange, column web, end-plate, and high-strength bolt. And, the initial stiffness could be calculated by the ratio between moment and rotation at the elastic ultimate stage.

As shown in Figure 10 and Table 7, in the elastic stage, the initial rotation stiffness and elastic ultimate moments of the spatial joints under planar loading were almost identical to those under spatial loading. The maximum error of the initial rotation stiffness of the spatial corner column joints under different loading modes corresponded to 1.8%. However, the middle column joints and the edge column

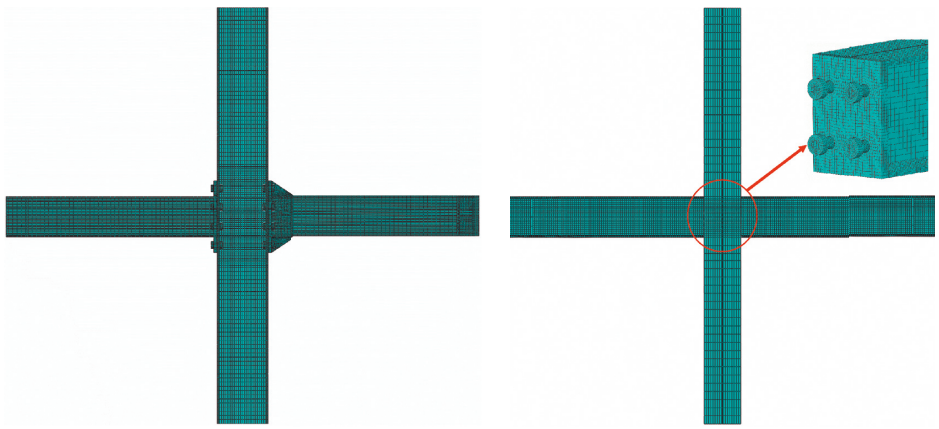

(a) (b)

Figure 5: FE model and mesh division. (a) Major-axis connection. (b) Minor-axis connection.

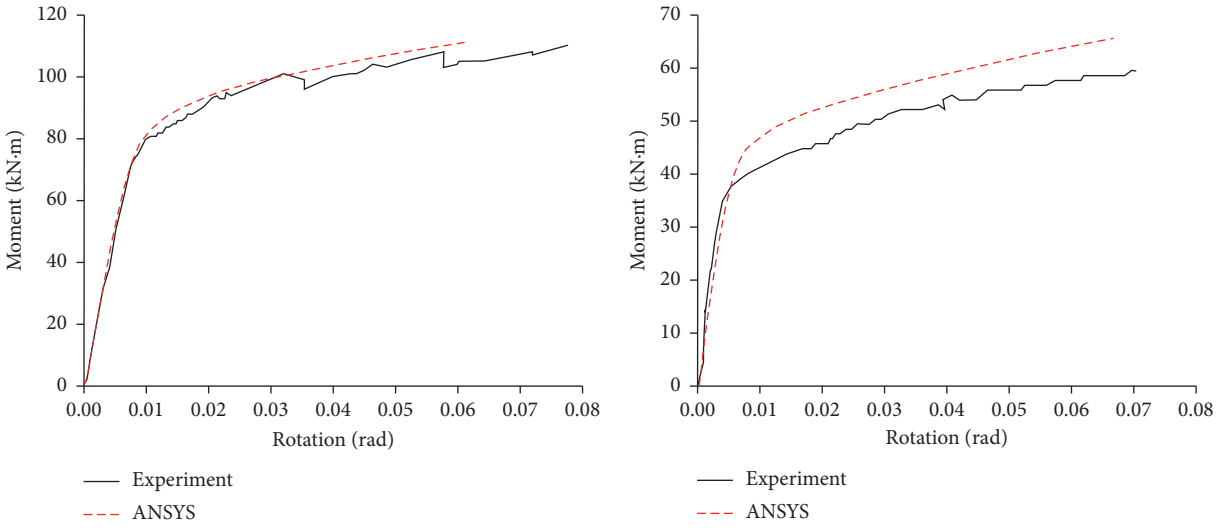

(a) (b)

Figure 6: Comparisons of the moment-rotation curves. (a) Specimen MZ-1. (b) Specimen MZ-2.

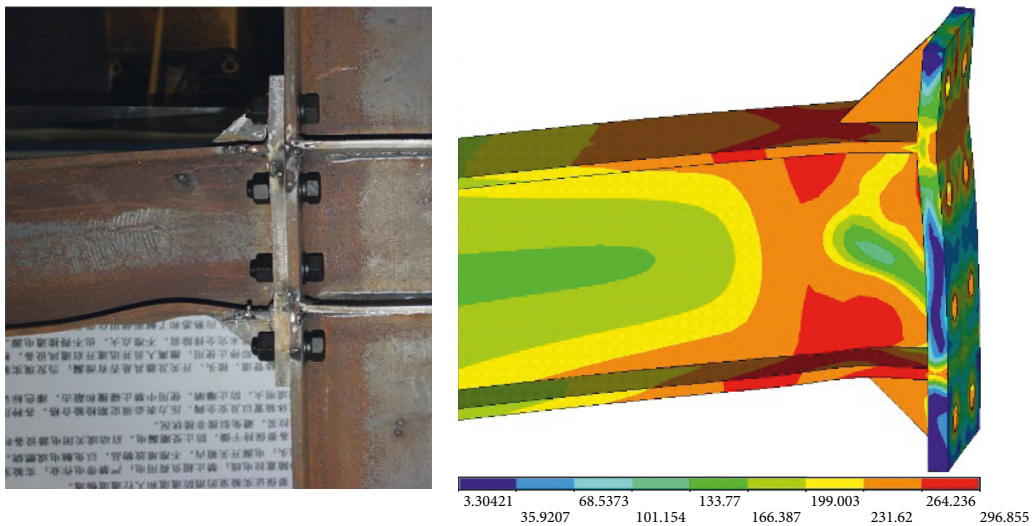

(a) (b)

Figure 7: Continued.

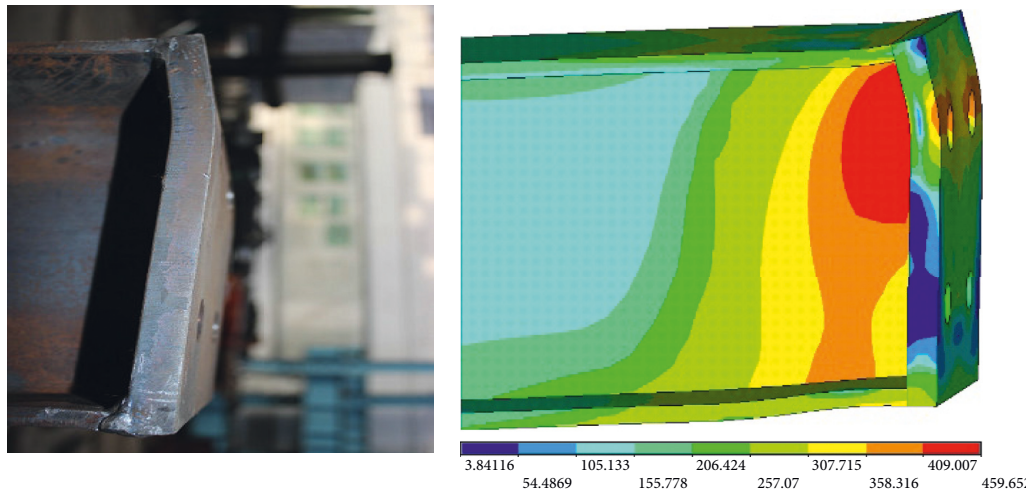

(c) (d)

Figure 7: Comparisons of the final deformation. (a) Right connection of MZ-1 in the test. (b) Right connection of MZ-1 in the FE model. (c) Left connection of MZ-2 in the test. (d) Left connection of MZ-2 in the FE model.

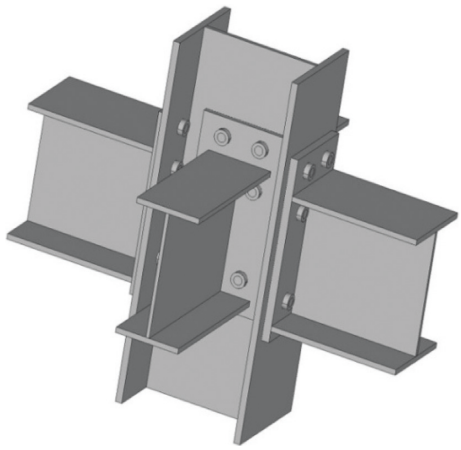

Figure 8: A spatial joint.

joints exhibited a greater difference in their bearing capacities under different loading modes. The joints under spatial loading yielded first, and then the plastic development was more rapid than that of the planar joints and the plastic region exceeded more than that of the planar joints. The bearing capacity of the joint under spatial loading was smaller than that under planar loading, and the maximum decrease of the corner column joints corresponded to 13%. The degradation of the bearing capacity of planar joints was slower than that of spatial joints. With respect to the middle column joints, the difference in the behaviour of the spatial load and that of the planar load was small.

Furthermore, as shown in Table 7, the initial stiffnesses of the middle column joints and edge column joints are larger than that of the corner column joints. With respect to the major-axis connection, the middle column joints and the edge column joints were under symmetric loading while the corner column joints were under unilateral loading. Hence, it was necessary to consider the effect of the shear deformation of the column web in the corner column joints which increased the relative rotation of the connection and reduced the rotation stiffness accordingly. The rotation stiffnesses of the middle column joints and the edge column joints were larger because it was not necessary to consider the effect of the shear deformation of the column web.

4. Initial Stiffness of Spatial Joints with End-Plate Connections

4.1. Flexural Stiffness of the Column Flange and End-Plate. An equivalent T-stub was considered to calculate the flexural stiffness of the column flange and the end-plate [21]. A very low level of prying force is produced by bolts in the elastic stage. Prying force usually occurs in the plastic stage, and it is a significant characteristic of the ultimate state of the joint [22]. Hence, it could be considered that the tightening effort of the bolt is continuous in the elastic stage, and based on this assumption, the bolted connection was assumed as a fixed connection and the prying action could be ignored. Figure 11 shows the mechanical model of the simplified equivalent T-stub.

The flexural stiffness of the column flange is calculated based on the theory of structural mechanics and material mechanics:

$$k_{\mathrm{cfb}} = \frac{2F}{\Delta} = 2 \times \frac{192\mathrm{EI}_{\mathrm{cf}}}{l_{\mathrm{cf}}^3} = \frac{32El_{\mathrm{eff,cf}}t_{\mathrm{cf}}^3}{l_{\mathrm{cf}}^3}, \tag{2}$$

where $I_{\mathrm{cf}} = (1/12) \cdot l_{\mathrm{eff,cf}} \cdot t_{\mathrm{cf}}^3$.

The flexural stiffness of the end-plate is expressed as follows:

$$k_{\mathrm{epb}} = \frac{2F}{\Delta} = 2 \times \frac{192\mathrm{EI}_{\mathrm{ep}}}{l_{\mathrm{ep}}^3} = \frac{32El_{\mathrm{eff,ep}}t_{\mathrm{ep}}^3}{l_{\mathrm{ep}}^3}, \tag{3}$$

where $l_{\mathrm{eff,cf}}$ and $l_{\mathrm{eff,ep}}$ denote the effective lengths of the equivalent T-stubs of the column flange and the end-plate, respectively, which are calculated by a method proposed by

(a) (b) (c)

Figure 9: FE models of the spatial joints. (a) YZ-1. (b) YZ-2. (c) YZ-3.

Table 5: Sizes of the planar joints.

Label	Column section (mm)	Beam in major axis (mm)	Beam in minor axis (mm)	End-plate thickness (mm)	Joint type	Note
PZ-1	H160 × 160 × 8 × 12	H240 × 120 × 6 × 9	—	14	Planar joint	1 major-axis beam
PZ-2	H160 × 160 × 8 × 12	H240 × 120 × 6 × 9	—	14	Planar joint	2 major-axis beam

Table 6: Sizes of the spatial joints.

Label	Column section (mm)	Beam in major axis (mm)	Beam in minor axis (mm)	End-plate thickness (mm)	Joint type	Note
YZ-1	H160 × 160 × 8 × 12	H240 × 120 × 6 × 9	H180 × 90 × 5 × 8	14	Corner column	1 major-axis beam, 1 minor-axis beam
YZ-2	H160 × 160 × 8 × 12	H240 × 120 × 6 × 9	H180 × 90 × 5 × 8	14	Edge column	2 major-axis beam, 1 minor-axis beam
YZ-3	H160 × 160 × 8 × 12	H240 × 120 × 6 × 9	H180 × 90 × 5 × 8	14	Middle column	2 major-axis beam, 2 minor-axis beam

Faella et al. [23]. The determined value is shown in Figure 12. Table 8 presents the values of $l_{\mathrm{eff,cf}}$ and $l_{\mathrm{eff,ep}}$. Additionally, t_{cf} and t_{ep} represent the thickness of the column flange and the end-plate, respectively.

Furthermore, d_m in Figure 12 denotes the effective diameter of the bolt head, and it is calculated as $d_m = 1.5d_{\mathrm{b}}$ where d_{b} denotes the nominal diameter of the bolt. Moreover, e denotes the distance between the centre of the bolt and the outer edge of the end-plate or the column flange, m denotes the distance between the bolt axis and the weld foot of the beam flange or the minor-axis connection plate, h_{e} denotes the effective height of the welded seam, and r_{c} denotes the radius of the web-to-flange fillet of the column.

4.2. Tension and Compression Stiffness of the Column Web. Partial areas between the minor-axis bolts are subject to minor tension and compression forces and involve low elastic strain in the compressive and tensile regions. These components were ignored when compared with the other components that are in high stress. Additionally, the decrease in the calculation height of the column web led to the increase in the initial stiffness of these joints. With respect to the effect of the thickness of the column web, the spread angle of the stress that is transferred from the bolt-hole edge to the centre of the column web was assumed as θ, and its values are presented in equation (4). The areas of the ignored parts of the compressive and tensile regions were then calculated, and the corresponding illustration of the calculation is shown in Figure 13. Table 9 presents the calculated results where d_{b} in the table denotes the nominal diameter of the bolt, and the definitions of other symbols can be found in Figure 13.

$$\text{For } t_{\mathrm{rep}} < 2t_{\mathrm{cw}}, \quad \theta = 45^{\circ}, \tag{4a}$$

$$\text{For } t_{\mathrm{rep}} > 2t_{\mathrm{cw}}, \quad \theta = 60^{\circ}, \tag{4b}$$

where t_{rep} is the thickness of the minor-axis end-plate and t_{cw} is the thickness of the web.

Where c is the transverse bolt pitch of the up flange along the minor-axis, d is the longitudinal bolt pitch of the up flange along the minor-axis, s is the distance from the bolt-hole center of the bottom flange to the bottom flange center.

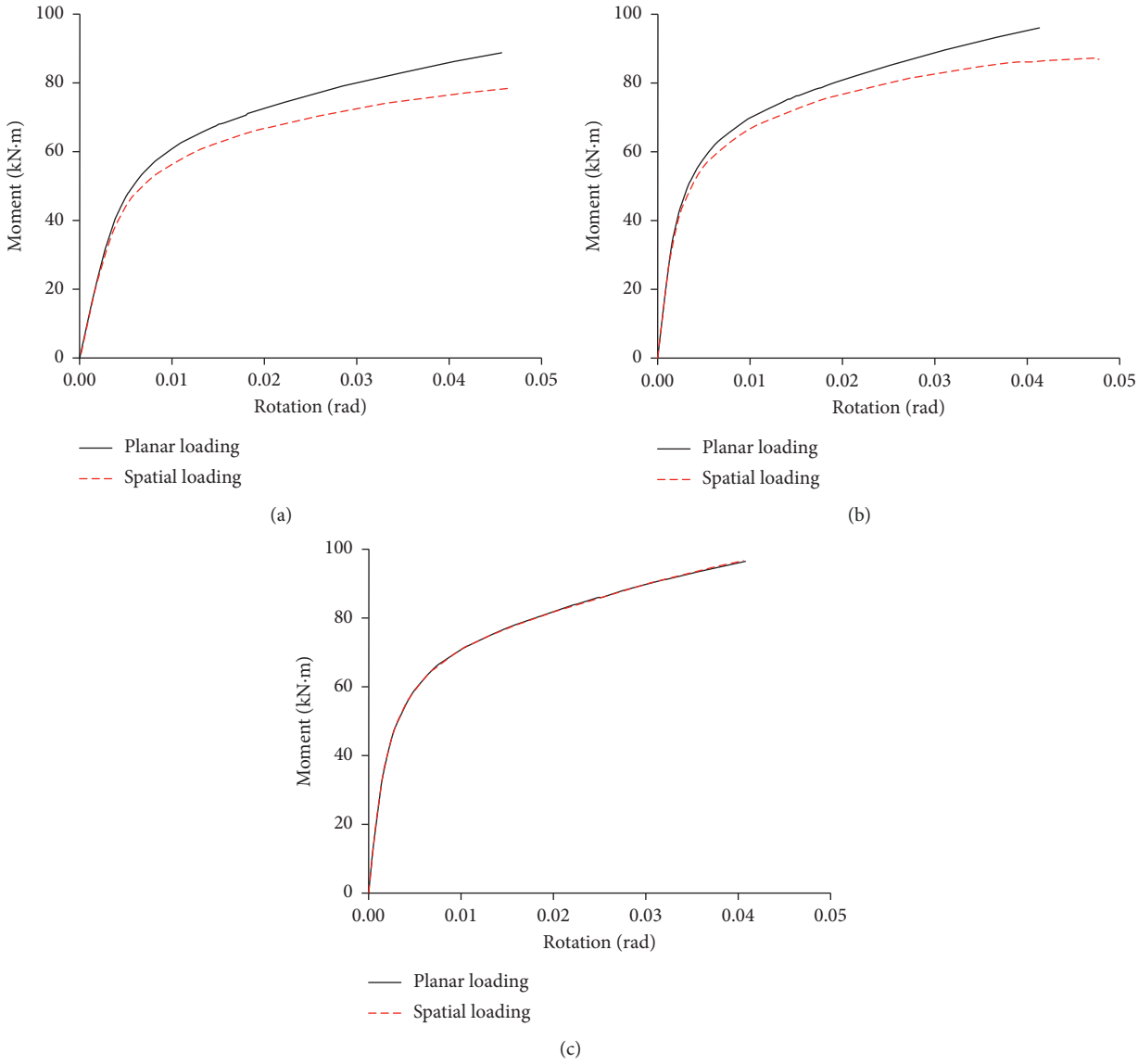

Figure 10: Moment-rotation curves of the spatial FE model under different loading modes. (a) YZ-1. (b) YZ-2. (c) YZ-3.

Table 7: Mechanical properties of the spatial joints.

Label	Elastic ultimate moments M (kN·m)		Initial rotation stiffness K_i (kN·m·rad^{-1})			Plastic ultimate moments M_u (kN·m)		
	Planar loading M_{e1}	Spatial loading M_{e2}	Planar loading K_1	Spatial loading K_2	K_1/K_2	Planar loading M_{u1}	Spatial loading M_{u2}	M_{u1}/M_{u2}
YZ-1	18.96	15.63	12837	13068	1.018	89.43	77.58	0.87
YZ-2	20.99	18.16	25520	25815	1.011	98.14	88.89	0.91
YZ-3	21.58	21.37	26764	26770	1.000	97.09	97.26	1.00

In the table, if the column is made of hot-rolled H steel, then $b_{eff,c} = t_{bf} + 2h_{e,ep} + 2t_{ep} + 2(t_{cf} + r_c)$. However, if the column is made of welded H steel, $b_{eff,c} = t_{bf} + 2h_{e,ep} + 2t_{ep} + 2(t_{cf} + h_{e,c})$, where $h_{e,ep}$ and $h_{e,c}$ denote the effective heights of welded seams of the end-plate and column, respectively. Additionally, r_c denotes the radius of the web-to-flange fillet of the column. The definitions of $h_{e,ep}$, $h_{e,c}$, t_{cf}, r_c, and t_{bf} are shown in Figure 14.

The principle of equivalent volume states that the ignored volume of the column web equals the decreased volume of the tensile and compressive stiffness components. According to this principle, the equivalent calculation height of the column web in tension or compression is calculated as follows:

$$h_{cw,t} = h_{cw} - \frac{S_t}{b_{eff,t}}, \tag{5a}$$

$$h_{cw,c} = h_{cw} - \frac{S_c}{b_{eff,c}}, \tag{5b}$$

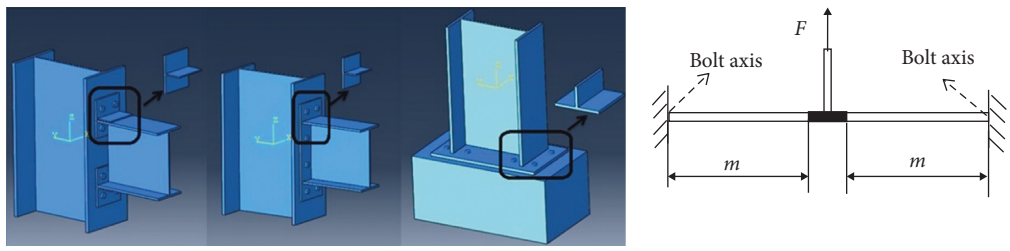

Figure 11: Mechanical model of the simplified equivalent T-stub. (a) The transformation of T-stub. (b) Simplified equivalent T-stub.

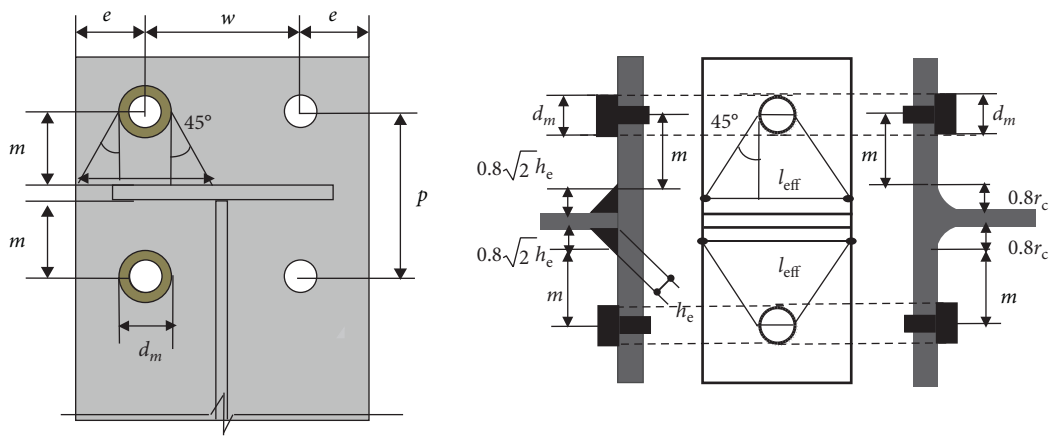

Figure 12: Calculation sketch of l_{eff}.

Table 8: Effective length of the equivalent T-stub.

T-stub type	Value
The effective lengths of the equivalent T-stub of end-plate $l_{eff,ep}$	$\min\{2m + d_m;\ m + e + d_m/2;\ m + w/2 + d_m/2;\ m + w/2 + e\}$
The effective lengths of the equivalent T-stub of column flange $l_{eff,cf}$	$\min\{2m + d_m;\ m + e + d_m/2;\ m + w/2 + d_m/2;\ m + w/2 + e\}$

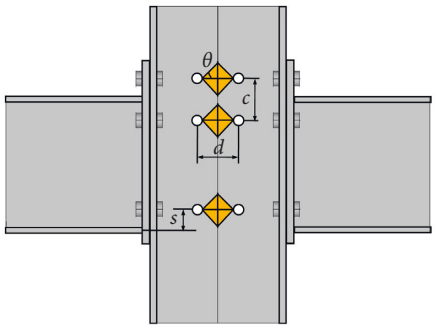

Figure 13: An illustration of the calculation of ignored parts of the column web.

where h_{cw} denotes the calculation height of the column web that is given as follows:

$$\begin{aligned} &\text{hot-rolled H steel column: } h_{cw} = h_c - 2\left(t_{cf} + r_c\right), \\ &\text{welded H steel column: } h_{cw} = h_c - 2\left(t_{cf} + h_{e,c}\right). \end{aligned} \tag{6}$$

The tensile and compressive stiffness of the column web can be calculated by simplifying the column web as axial tension and axial compression plates. Furthermore, it is necessary to consider the effect of different loading modes on the stiffness of the joint.

The compressive stiffness of the column web is calculated as follows:

$$k_{cwc} = \frac{Eb_{eff,c}t_{cw}}{\varphi h_{cw,c}}, \tag{7}$$

where $h_{cw,c}$ denotes the equivalent calculation height of the column web in compression; t_{cw} denotes the thickness of the column web; and $b_{eff,c}$ denotes the effective height of the column web in compression. According to Eurocode 3 [16], φ denotes the influence coefficient of load and corresponds to 0.5 for symmetric loads, 1 for antisymmetry loads, and 1 for other loads.

The compressive stiffness of the column web is expressed as follows:

Table 9: Calculation of the ignored area of the column web.

Tensile region of the column web		Compressive region of the column web	
Condition for ignored tensile area	Ignored tensile area S_t	Condition for ignored compressive area	Ignored compressive area S_c
$(d-d_b)\tan\theta c$	$0.5\{(d-d_b)^2\tan\theta+d_b^2\}$	$s0.5\{b_{eff,c}-(d-d_b)\tan\theta\}$	$0.5\{(d-d_b)^2\tan\theta+d_b^2\}$
$(d-d_b)\tan\theta c$	$0.25\{c(2d-2d_b-c\cot\theta)+2d_b^2+(d-d_b)^2\tan\theta\}$	$s0.5\{b_{eff,c}-(d-d_b)\tan\theta\}$ $s0.5\{b_{eff,c}+(d-d_b)\tan\theta\}$ $s0.5\{b_{eff,c}+(d-d_b)\tan\theta\}$	$0.25\{(d-d_b)^2\tan\theta+d_b^2\}$ 0

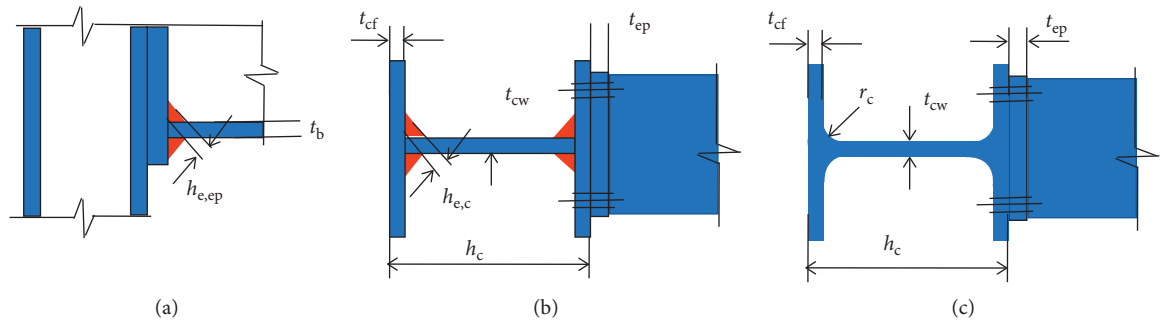

Figure 14: Sizes of the column web. (a) Front view of the welded joint. (b) Top view of the welded joint. (c) Top view of the hot-rolled joint.

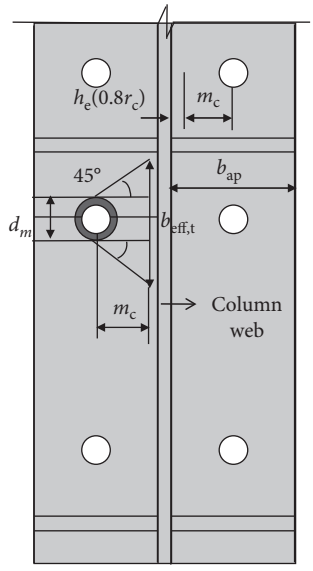

Figure 15: Calculation sketch of the effective tensile width of the column web.

Table 10: Value of effective tensile width.

Criterion	Value of effective tensile width
$m_c(p-d_m)/2$	$b_{eff,t}2m_c+d_m$
$m_c(p-d_m)/2$	$b_{eff,t}m_c\tan 45^\circ+(d_m+p)/2$

$$k_{cwt}=\lambda\frac{Eb_{eff,t}t_{cw}}{\varphi h_{cw,t}}, \tag{8}$$

where $h_{cw,t}$ denotes the equivalent calculation height of the column web in tension. This is equal to $\lambda(p/w)^3$ based on the principle that states that the distribution of the tension of the bolts depends on the stiffness of the column web and the minor-axis connection plate in conjunction with the principle that states that the column web and the minor-axis connection plate as shown in the present study have the same equivalent tensile deformation. Additionally, λ denotes the influence coefficient of bolt spacing. Each parameter is illustrated in Figure 12. The effective tensile width is shown in Figure 15, and its values are listed in Table 10.

4.3. Tensile Stiffness of Bolts. The study ignored the effect of the prying force of the bolts in the rotation stiffness calculation. Additionally, it was necessary to modify the suggested formula of the Eurocode to calculate the tensile stiffness of the bolts. Furthermore, the coefficient γ was introduced into the calculation model for high-strength bolts based on the effect of prestress. The value of γ is based on a previous study [24] and generally corresponded to 10. The tensile stiffness of the bolts can then be derived as follows:

$$k_{bt}=2(1+\gamma)\frac{EA_s}{L_b}, \tag{9a}$$

$$L_b=t_{ep}+t_{cf}+2t_{wh}+\frac{t_h+t_n}{2}, \tag{9b}$$

where A_s denotes the effective area of the bolt rod and is typically (in engineering) equal to 0.8 times the nominal area of the rod. L_b denotes the calculation length of the bolt. The meaning of thickness variation t can be found in the appendix.

4.4. Modification of the Rotation Stiffness Calculation Model of the Spatial Joints. The deformation of the upper connection includes the deformation of the bolts, end-plates, the bending deformation of column flanges, and tensile deformation of the column web. The deformation of the lower

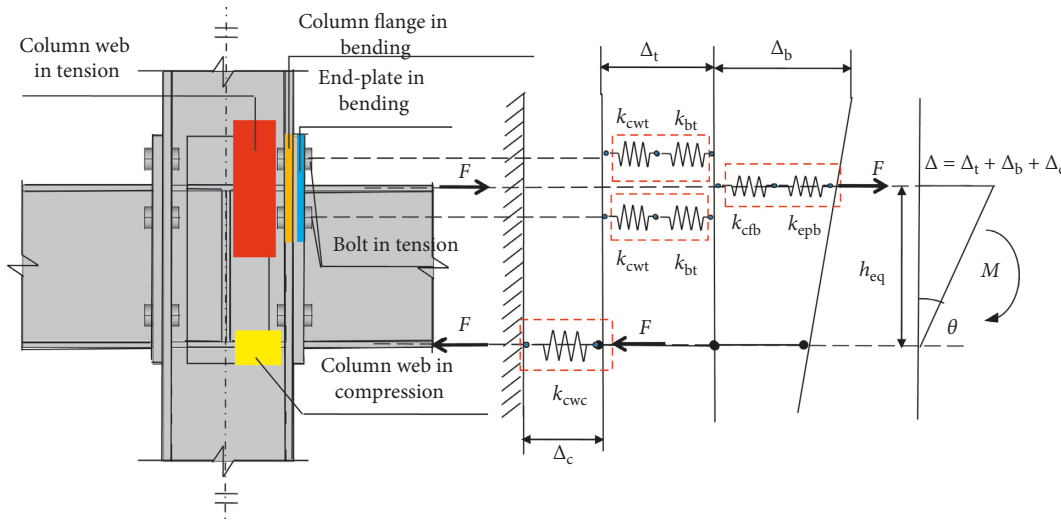

Figure 16: Calculation model of the rotation stiffness of the spatial middle column joint.

Table 11: Geometric properties of the spatial joints.

Sizes of beam and column (mm)		The major-axis end-plate type	Joint label	The minor-axis end-plate sizes (mm) Spacing d	Distance n	Diameter Φ	End-plate thickness t	The minor-axis end-plate type
C-series	Column H200 × 200 × 8 × 12 The major-axis beam H250 × 150 × 6 × 9 The minor-axis beam H250 × 125 × 6 × 9 The major-axis end-plate 340 × 150 × 14	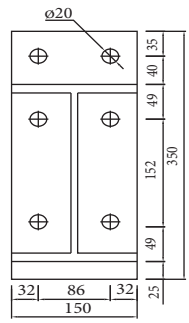	C01	66	40	20	12	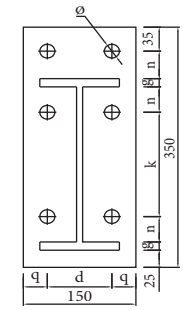
			C02	76	40	16	12	
			C03	76	40	24	12	
			C04	86	40	20	12	
			C05	86	40	20	20	
			C06	106	40	20	12	
D-series	Column H300 × 250 × 10 × 15 The major-axis beam H300 × 200 × 8 × 12 The minor-axis beam H300 × 150 × 8 × 12 The major-axis end-plate thickness 18	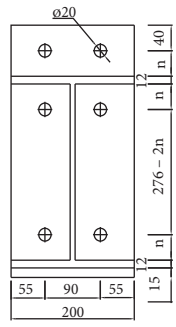	D01	70	40	20	12	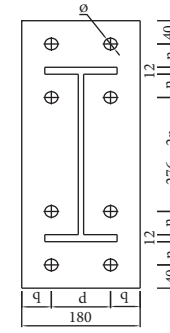
			D02	80	40	16	12	
			D03	90	40	20	12	
			D04	90	30	20	12	
			D05	120	40	20	12	
			D06	90	40	20	22	

flanges could be reflected by the compressive deformation of the column web. The connection was in accordance with the plane section assumption of the steel beam and the assumption that the rotational centre of the joint was located in the center of the lower flanges along the thickness direction. The initial rotation stiffness calculation model of the spatial middle column joint is illustrated in Figure 16.

The total deformation of the spatial middle column joints can be divided into three parts, namely, Δ_t that corresponds to the tensile deformation of the column web and bolts, Δ_b that corresponds to the bending deformation of the end-plate and column flange, and Δ_c that corresponds to the compressive deformation of the column web.

Table 12: Comparison results between the theoretical and FEM analysis.

Joint label	Initial rotation stiffness of the major-axis connection (kN·m/rad)		
	Theoretical result (T)	FEM result (F)	Error $(T-F)/F$ %
C01	29859	31617	−5.56
C02	31426	31686	−0.82
C03	31479	32603	−3.45
C04	31989	32686	−2.14
C05	33586	33879	−0.87
C06	33510	33220	0.87
D01	57831	60474	−4.37
D02	59046	59662	−1.03
D03	60413	61483	−1.74
D04	54576	65031	−16.07
D05	66599	63448	4.97
D06	64676	61791	4.67

Based on the above assumptions, the rotation of the joint in the elastic range is given by the following expression:

$$\theta = \frac{\Delta_t + \Delta_b + \Delta_c}{h_{eq}} = \frac{F}{h_{eq}}\left(\frac{1}{2k_{cwt}} + \frac{1}{2k_{bt}} + \frac{1}{k_{cfb}} + \frac{1}{k_{epb}} + \frac{1}{k_{cwc}}\right), \tag{10}$$

where h_{eq} denotes the equivalent calculation height with a value that is equal to the distance between the centre of the upper flange of the beam and the rotational centre, and it can be expressed as $h_{ep} = h_b - t_{bf}$ where h_b denotes the height of the beam.

The calculation of the initial rotation stiffness of the joint is as follows:

$$K_{ini} = \frac{Fh_{eq}}{\theta} = \frac{h_{eq}^2}{(1/2k_{cwt}) + (1/2k_{bt}) + (1/k_{cfb}) + (1/k_{epb}) + (1/k_{cwc})}. \tag{11}$$

4.5. Verification of the Rotation Stiffness Calculation Model of the Spatial Joints. Several FE models were built to verify the accuracy of equation (11). The specific forms and sizes of joints are specified in Table 11. For spatial joints of C series, the form of the major-axis connection remains unchanged; the variable parameters along the minor axis include the thickness of the end-plate, the bolt pitch, and the bolt diameter. The minor axis connections of D series are in different forms. The end-plate was extended at both ends, while the variable parameters along the minor axis include end-plate thickness, bolt-hole diameter, and bolt pitch. Comparisons between results by the theoretical analysis and results by FEM analysis are listed in Table 12.

As shown in Table 12, the results between theoretical calculation and FEM analysis results are in good accordance for most of the spatial joints, with errors less than ±5%. While for few of the joints, the relatively larger errors occurred due to the poor design of bolt spacing, such as for joint D04, there is a large bolt spacing difference between the vertical and horizontal axis. So generally, the theoretical equation proposed in this article is of good applicability for most reasonably designed joints.

5. Conclusion

This study involved analyzing the interaction between the major axis and the minor axis of spatial joints and the differences in the performances of the spatial joints and planar joints. Finally, a calculation equation for the initial rotation stiffness of spatial joints was presented based on the component method. The key conclusions of the study include the following:

(i) The rotation stiffness of spatial joints under spatial loading typically exceeded that under planar loading. However, the bending moments of the spatial joints under spatial loading were lower than those under symmetric planar loading.

(ii) The initial rotation stiffness and bearing capacity of the spatial joints were significantly higher than those of the planar joints. Mechanical performances between the spatial joints and planar joints are different. The components that contributed to the stiffness of the spatial joints were analysed to derive the stiffness calculation formula of each component based on elastic theory. Additionally, the stiffness of the specific components of the spatial joints was calculated, and compared with the FEM results, a relatively accurate formula of stiffness was presented.

(iii) The calculation model and the theoretical equation of the initial rotation stiffness of joints were rebuilt based on the sources of the deformation of the joints. Furthermore, the accuracy of the calculation formula presented in this study was verified based on calculation examples and several FE models.

Nomenclature

A_s: The effective area of the bolt rod
$b_{eff,c}$: The effective height of the column web in compression
db: The nominal diameter of the bolt
d_m: The effective diameter of the bolt head
E: Elasticity modulus
f_u: Tensile stress
f_y: Yield stress
h_b: The height of the beam
h_{cw}: The calculation height of the column web
$h_{cw,c}$: The equivalent calculation height of the column web in compression
$h_{cw,t}$: The equivalent calculation height of the column web in tension
h_e: The effective height of the welded seam
$h_{e,c}$: The effective heights of welded seams of the column
$h_{e,ep}$: The effective heights of welded seams of the end-plate
I_T: The cross-sectional moment of inertia
K_i: Initial rotation stiffness

k_{tn}: The tensile stiffness in the height of each row of bolts
L_b: The calculation length of the bolt
$l_{eff,cf}$: The effective lengths of the equivalent T-stubs of the column flange
$l_{eff,ep}$: The effective lengths of the equivalent T-stubs of the end-plate
l_T: The calculation span of T-stub
M: Elastic ultimate moments
M_u: Plastic ultimate moments
m: The distance between the bolt axis and the weld foot of the beam flange
r_c: The radius of the web-to-flange fillet of the column
t_{cf}: Thickness of the column flange
t_{cw}: The thickness of the web
t_{ep}: The thickness of the end-plate
t_h: Thickness of the bolt head
t_n: The thickness of the bolt nut
t_{rep}: The thickness of the minor-axis end-plate
t_{wh}: The thickness of the gasket
Δb: The bending deformation of the end-plate and column flange
Δc: The compressive deformation of the column web
Δt: The tensile deformation of the column web and bolts
ε_y: Yield strain
λ: The influence coefficient of bolt spacing
φ: The influence coefficient of the load.

Data Availability

All the data used to support the findings of this study have been deposited in the figshare repository (https://figshare.com/s/da80ea5e386b41b4c092). They are available from the first author upon request.

Conflicts of Interest

The authors declare that they have no conflicts of interest.

Acknowledgments

This study was supported by the National Natural Science Foundation of China (grant nos. 51778241; 51708226; 51638009; and 51978279), by the State Key Laboratory of Subtropical Building Science of South China University of Technology (grant nos. 2018ZB35, 2017ZB28, and 2017KD22), and by the Fundamental Research Funds for the Central Universities (Grant nos. 2017BQ086 and 2019ZD47).

References

[1] M. M. Tahir, M. A. Hussein, A. Sulaiman, and S. Mohamed, "Comparison of component method with experimental tests for flush end-plate connections using hot-rolled perwaja steel sections," *International Journal of Steel Structures*, vol. 9, no. 2, pp. 161–174, 2009.

[2] M. Pecce, F. Rossi, F. A. Bibbo, and F. Ceroni, "Experimental behaviour of composite beams subjected to a hogging moment," *Steel & Composite Structures*, vol. 12, no. 5, pp. 395–412, 2012.

[3] R. Tartaglia, M. D'Aniello, G. A. Rassati, J. A. Swanson, and R. Landolfo, "Full strength extended stiffened end-plate joints: AISC vs recent European design criteria," *Engineering Structures*, vol. 159, pp. 155–171, 2018.

[4] R. Tartaglia, M. D'Aniello, and R. Landolfo, "The influence of rib stiffeners on the response of extended end-plate joints," *Journal of Constructional Steel Research*, vol. 148, pp. 669–690, 2018.

[5] A. B. Francavilla, M. Latour, V. Piluso, and G. Rizzano, "Design of full-strength full-ductility extended end-plate beam-to-column joints," *Journal of Constructional Steel Research*, vol. 148, pp. 77–96, 2018.

[6] V. Katalin and I. Miklós, "Investigation of minor axis and 3D bolted end-plate connections-experimental and numerical analysis-load tests," *Periodicapolytechnicaser*, vol. 49, no. 1, pp. 47–58, 2005.

[7] J. M. Cabrero and E. Bayo, "The semi-rigid behaviour of the three-dimensional steel beam-to-column joints subjected to proportional loading. Part I: experimental evaluation," *Journal of Constructional Steel Research*, vol. 63, no. 9, pp. 1241–1253, 2007.

[8] J. M. Cabrero and E. Bayo, "The semi-rigid behaviour of the three-dimensional steel beam-to-column joints subjected to proportional loading. Part II: theoretical model and validation," *Journal of Constructional Steel Research*, vol. 63, no. 9, pp. 1254–1267, 2007.

[9] L. Simões da Silva, "Towards a consistent design approach for steel joints under generalized loading," *Journal of Constructional Steel Research*, vol. 64, no. 9, pp. 1059–1075, 2008.

[10] A. Loureiro, A. Moreno, R. Gutiérrez, and J. M. Reinosa, "Experimental and numerical analysis of three-dimensional semi-rigid steel joints under non-proportional loading," *Engineering Structures*, vol. 38, pp. 68–77, 2012.

[11] B. Gil, R. Goñi, and E. Bayo, "Experimental and numerical validation of a new design for three-dimensional semi-rigid composite joints," *Engineering Structures*, vol. 48, pp. 55–69, 2013.

[12] H. Zhou, "Experimental and theoretical study on 3D composite joints under bidirectional loading," Doctoral thesis, Tsinghua University, Beijing, China, 2011.

[13] S. Z. Chen, J. R. Pan, H. Yuan, Z. N. Xie, Z. Wang, and X. Dong, "Mechanical behaviour investigation of steel connections using a modified component method," *Steel and Composite Structures*, vol. 25, no. 1, pp. 117–126, 2017.

[14] Ž. Bučmysa, A. Daniūnasa, J. P. Jaspartb, and J. F. Demonceaub, "A component method for cold-formed steel beam-to-column bolted gusset plate joints," *Thin-Walled Structures*, vol. 123, pp. 520–527, 2018.

[15] N. H. R. Sulong, A. Y. Elghazouli, B. A. Izzuddin, and N. Ajit, "Modelling of beam-to-column connections at elevated temperature using the component method," *Steel and Composite Structures*, vol. 10, no. 1, pp. 23–43, 2010.

[16] CEN, *Eurocode 3. Eurocode 1993-Design of Steel Structures -Part 1-8: Design of Joints and Building Frames*, CEN, Brussels, Belgium, 2005.

[17] China Planning Press, *Code for Design of Steel Structure*, China Planning Press, Beijing, China, 2003.

[18] B. Guo, "Collapse mechanism and design criterion of steel beam-to-column end-plate connections under cyclic load," Doctoral thesis, Xi'an University of Architecture and Technology, Xi'an, China, 2002.

[19] Z. Wang and T. Wang, "Experiment and finite element analysis for the end plate minor axis connection of semi-rigid steel frames," *China Civil Engineering Journal*, vol. 45, no. 8, pp. 83–89, 2012.

[20] ANSYS Inc, *ANSYS Version 19.0 Documentation*, ANSYS Inc, Canonsburg, PA, USA, 2018.
[21] Z. Al-Khatab and A. Bouchaïr, "Analysis of a bolted T-stub strengthened by backing-plates with regard to Eurocode 3," *Journal of Constructional Steel Research*, vol. 63, no. 12, pp. 1603–1815, 2007.
[22] M. R. Bahaari and A. N. Sherbourne, "3D simulation of bolted connections to unstiffened columns II: extended endplate connections," *Journal of Constructional Steel Research*, vol. 40, no. 3, pp. 189–223, 1996.
[23] C. Faella, V. Piluso, and G. Rizzano, "Experimental analysis of bolted connections: snug versus preloaded bolts," *Journal of Structural Engineering*, vol. 124, no. 7, pp. 765–774, 1998.
[24] G. Q. Li, W. L. Shi, and J. F. Wang, *Design of Steel Frames with Semi-Rigid Connections*, China Building Industry Press, Beijing, China, 2009.